Monatshefte für Chemie 138, 1211–1215 (2007)
DOI 10.1007/s00706-007-0709-z
Printed in The Netherlands

Monatshefte für Chemie
Chemical Monthly

Thermal Analysis of the System Na_3AlF_6–$NaVO_3$

Marián Kucharík[1], **František Šimko**[1,*], **Vladimír Danielik**[2], **Miroslav Boča**[1], and **Roman Vasiljev**[1]

[1] Slovak Academy of Sciences, Institute of Inorganic Chemistry, Bratislava, Slovakia
[2] Faculty of Chemical and Food Technology, Institute of Inorganic Chemistry, Technology and Materials, Slovak University of Technology, Bratislava, Slovakia

Received December 20, 2006; accepted May 9, 2007; published online September 24, 2007

Summary. The phase diagram of the system Na_3AlF_6–$NaVO_3$ was determined by means of thermal analysis. The system is a simple binary eutectic one. The eutectic point was estimated at $x(NaVO_3) = 0.975$ and $t_{eut} = 617°C$. The XRD patterns of samples after thermal analysis revealed the presence of cryolite and $NaVO_3$ only supporting the above assumption of a simple eutectic binary system.

Keywords. Thermal analysis; Phase diagram; Vanadium impurities; Aluminum electrolysis.

Introduction

The industrial electrolyte of aluminum production (*Hall–Héroult* process) commonly contains impurities, like iron, silicon, sulphur, phosphorous, and vanadium, *etc.* [1]. The impurities are introduced to the aluminum cell mainly through the raw materials, which are alumina and fluoride salts, and through anodes [2]. Vanadium belongs to the harmful impurities causing the decrease in current efficiency [3].

Bratland et al. [4] measured the solubility of vanadium pentoxide in pure cryolite and in cryolite-alumina melts using the ''visual'' method. The solubility of V_2O_5 in pure molten cryolite at 1030°C was 1.1 *wt%* [4]. This result is in accordance with older measurements of *Rolin et al.* [5] and *Belyaev et al.* [6]. *Bratland et al.* [4] found that the solubility of vanadium decreased linearly with increasing alumina content in cryolite.

Goodes and *Algie* [7] investigated the distribution of vanadium impurities between bath and aluminum and between bath and gaseous phases. They detected residual vanadium in the bath, during the vanadium transfer across the bath/aluminum interface. Moreover, the content of vanadium in the bath was higher than reported by *Bratland et al.* [4]. The condensate from the fumes above the melt contained vanadium, particularly during the first 2–4 h of the runs, and then the volatilization seemed to cease. The reported differences can arise from the fact that different experimental conditions were considered.

Chrenková et al. [8] studied the system Na_3AlF_6-V_2O_5 by thermal analysis. These authors concluded that the solubility of vanadium pentoxide in pure cryolite is higher than reported in Refs. [4–6].

Besides the lowering of the current efficiency the vanadium impurities introduced into the bath have a negative influence on the quality of produced metal [1]. In spite of this fact, known for decades, no other data are available considering vanadium based impurities in the cryolite melts.

In this work, the behavior of $NaVO_3$ in the cryolite melt is investigated by means of thermal analysis. The reason for selection of this compound can be demonstrated in the following reaction:

$$1/2NaVO_3(l) + Al(l) = 1/2Al_2O_3(s) + 1/2V(s) + 1/2Na(l)$$
$$\Delta_r G^{O}_{1300\,K} = -242.5\,kJ\,mol^{-1}$$

* Corresponding author. E-mail: uachsim@savba.sk

This reaction explains the reason of current efficiency decrease during the aluminum electrolysis as a consequence of back oxidation of aluminum. Moreover, the value of $\Delta_r G^O$ of this reaction is comparable to the reaction of aluminum with vanadium pentoxide [4] which makes both reactions competitive in terms of reaction energy:

$$3/10V_2O_5(l) + Al(l) = 1/2Al_2O_3(s) + 3/5V(s)$$
$$\Delta_r G^O_{1300\,K} = -326.0\,kJ\,mol^{-1}$$

Results and Discussion

The number of species originating from a substance B added to a molten salt A can be determined from the equation for freezing point depression (Eq. (1)),

$$\Delta_{fus}T_A = \frac{RT^2_{fus,A}}{\Delta_{fus}H_A}x_B k_{St} \qquad (1)$$

where R is the gas constant, $T_{fus,A}$ and $\Delta_{fus}H_A$ are the temperature and enthalpy of fusion of the solvent A, x_B is the mole fraction of the solute B, and k_{St} is the *Stortenbeker* factor, which equals the number of new foreign species being introduced by the solute B into the solvent A [9]. Differentiating Eq. (1) according to x_B and setting for $x_A \rightarrow 1$ the relation for the tangent to the liquidus curve of the solvent A (reduced for the temperature of melting of pure solvent), k_0, is obtained:

$$\lim_{x_A \rightarrow 1}\left(\frac{d(\Delta_{fus}T_A)}{dx_B}\right) = \frac{RT^2_{fus,A}}{\Delta_{fus}H_A}k_{St} = k_0 \qquad (2)$$

Knowing $\Delta_{fus}T_A$ and $\Delta_{fus}H_A$ the *Stortenbeker* factor[a] k_{St} can be calculated. More precisely, the concept of *Stortenbeker* factor should be interpreted as number of moles of reaction products (excluding the reaction products of dissociation reactions of the solvent) that are produced by addition of 1 mol of solute B to an infinite (huge) amount of solvent A. More details on description of definition of number of foreign species introduced to the solution having dystectic melting mode (*e.g.* cryolite) can be found in works by *Šimko et al.* [10] and *Proks et al.* [11].

[a] Identical to the *van't Hoff* factor in solution chemistry, see Lewis G. N., Randall M., *Thermodynamics*, 2nd ed., McGraw-Hill, New York, NY, revised by Pitzer K. S., Brewer L. (1961) p. 220 and 301

The calculation of the phase diagrams of the condensed systems using the coupled analysis of the thermodynamic and phase diagram data is based on the solution of a set of equations of the following type, where each of the equation describes the field of primary crystallization of the component i:

$$\Delta_{fus}G^O_i(T) + RT\ln\frac{a_{l,i}(T)}{a_{s,i}(T)} = 0 \qquad (3)$$

$\Delta_{fus}G^O_i$ is the standard molar *Gibbs* energy of fusion of the component i at the temperature T, R is the gas constant, and $a_{s,i}(T)$ and $a_{l,i}(T)$ are the activities of the component i in the solid and liquid phase at the temperature T. The molar excess *Gibbs* energy of mixing in the liquid phase of the binary system was described by the following general equation:

$$\Delta G^E_{bin} = \sum_{j=1} x_1 x_2^j G_j \qquad (4)$$

G_j is a coefficient of interaction. It is supposed, that parameter G_j does not depend on the composition and in the field interesting for the investigation of the phase diagram the molar excess *Gibbs* energy of mixing is independent from the temperature.

The coupled thermodynamic analysis, *i.e.* the calculation of the coefficients G_j in Eq. (3) has been performed using multiple linear regression analysis omitting the statistically non-important terms in the excess molar *Gibbs* energy of mixing on the 0.98 confidence level according to the Student t-test. As the optimizing criterion for the best fit between the experimental and calculated temperatures of the primary crystallization the following condition was used for all measured points

$$\sum_n (T_{pc,exp,n} - T_{pc,calc,n})^2 = \min \qquad (5)$$

The values of the enthalpy and temperature of fusion of individual components used in the calculation of coefficients G_j or *Stortenbeker* factor are summarized in Table 1.

The experimentally determined and calculated results are presented in Table 2.

Table 1. Values of the enthalpy and temperature of fusion

Component	T_{fus}/K	$\Delta_{fus}H$/kJ mol^{-1}
Na_3AlF_6	1284 [12]	106.745 [12]
$NaVO_3$	903 [13]	28.326 [13]

Table 2. Compositions, experimental, t_{pc}(exp), calculated, t_{pc}(calc), temperatures of primary crystallization; their differences, Δt; and eutectic temperatures, t_{eut}(exp), in the system Na_3AlF_6–$NaVO_3$

$x(NaVO_3)$	t_{pc}(exp)/°C	t_{pc}(calc)/°C	Δt/°C	t_{eut}(exp)/°C	Crystallizing phase
0.0000	1011.0	1011.0	0		Na_3AlF_6
0.0075	1010.4	1010.1	0.3		Na_3AlF_6
0.0100	1008.9	1009.8	−0.9		Na_3AlF_6
0.0150	1007.1	1009.2	−2.1		Na_3AlF_6
0.0200	1007.2	1008.6	−1.3		Na_3AlF_6
0.0300	1006.1	1007.5	−1.4		Na_3AlF_6
0.0300	1004.6	1007.5	−2.9		Na_3AlF_6
0.0350	1005.7	1006.9	−1.2		Na_3AlF_6
0.0375	1005.4	1006.6	−1.2		Na_3AlF_6
0.0400	1002.5	1006.4	−3.9		Na_3AlF_6
0.0500	1001.3	1005.3	−4.0		Na_3AlF_6
0.1000	994.5	1000.2	−5.8		Na_3AlF_6
0.1000	996.4	1000.2	−3.6		Na_3AlF_6
0.1500	991.5	994.9	−3.4		Na_3AlF_6
0.2000	989.0	989.2	−0.2		Na_3AlF_6
0.2500	982.2	982.9	−0.7		Na_3AlF_6
0.3000	978.4	976.3	2.1		Na_3AlF_6
0.4000	963.8	963.3	0.5		Na_3AlF_6
0.5000	955.3	952.1	3.2		Na_3AlF_6
0.6000	942.0	941.7	0.3	616	Na_3AlF_6
0.7000	920.0	924.9	−4.9	619	Na_3AlF_6
0.8000	884.0	884.8	−0.8	619	Na_3AlF_6
0.9000	789.2	788.4	0.8	615.3	Na_3AlF_6
0.9500	703.4	696.1	7.3	620	Na_3AlF_6
0.9750	617	623.1	−6.1	617	eut. mixture
1.0000	630	630	0		$NaVO_3$

The calculated phase diagram of the system Na_3AlF_6–$NaVO_3$ together with experimental data is shown in Fig. 1. In these composition coordinates the system is a simple binary eutectic one. The XRD patterns of samples after thermal analysis revealed the presence of cryolite and $NaVO_3$ only supporting the above assumption of a simple eutectic binary system. The eutectic point was estimated at $x(NaVO_3) = 0.975$ and $t_{eut} = 617$°C. The calculated eutectic point of this binary system is at $x(NaVO_3) = 0.976$ and $t_{eut} = 623$°C.

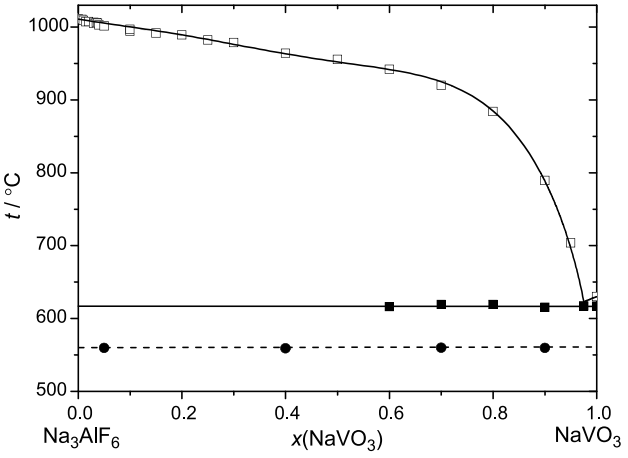

Fig. 1. Phase diagram of the system Na_3AlF_6-$NaVO_3$, □ – primary crystallization data, ■ – solidus data, ● – phase transition of Na_3AlF_6 (560 ± 2°C), full line – calculated

The calculation of the phase diagram of the system Na_3AlF_6–$NaVO_3$ has been performed for a simple eutectic binary system. The chemical reactions were not considered in the calculation, these are not known. In this case the possible chemical reactions are involved in activity coefficients which characterize non-ideal behaviour of the system.

The following equation of the composition dependence of the molar excess *Gibbs* energy has been obtained for the system Na_3AlF_6–$NaVO_3$:

$$\Delta G^{E}_{BIN} = x_1 x_2 (G_0 + G_1 x_2 + G_2 x_2^2 + G_3 x_2^3)$$
$$x_1 = x(Na_3AlF_6), \quad x_2 = x(NaVO_3) \qquad (6)$$

The values of interaction coefficients G_j are given in Table 3. The standard deviation of the approximation is $SD \pm 3.17$°C.

Table 3. Values of interaction coefficients G_j

Coefficients	G_j/kJ mol^{-1}	SD/kJ mol^{-1}
G_0	10.21	1.68
G_1	−25.14	8.98
G_2	61.20	15.91
G_3	−54.59	8.94

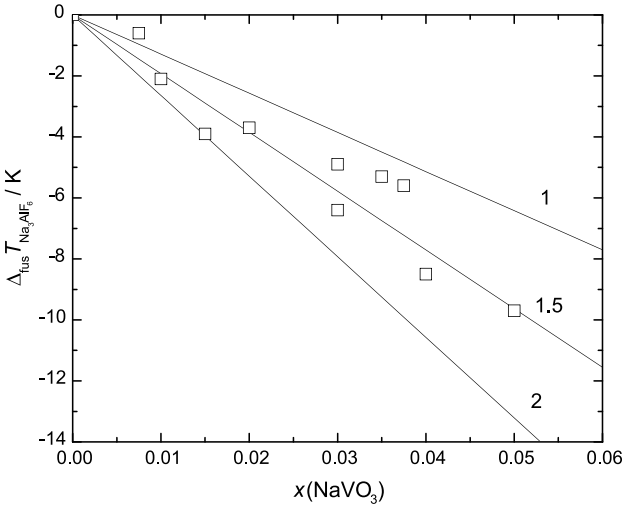

Fig. 2. Freezing point depression, $\Delta_{fus}T_{Na_3AlF_6}$, as a function of the mole fraction of $NaVO_3$ from 0 up to 0.05. Full lines: Freezing point depression curves for three different *Stortenbeker* factor values (1, 1.5, and 2)

From the composition interval within $x(NaVO_3) =$ 0–0.05 the linear fit of $\Delta_{fus}T_{Na_3AlF_6}$ (Eq. (2)) provided $k_0 = 184.4 \pm 9.0$. Since the enthalpy of fusion and the temperature of fusion for pure cryolite are known, the calculated *Stortenbeker* factor, k_{St}, according to Eq. (2) is equal to 1.45 ± 0.07. In Fig. 2 three lines corresponding to three different *Stortenbeker* factor values (1, 1.5, and 2) are plotted together with experimental data within $x(NaVO_3) = 0$–0.05. It can be expected that $NaVO_3$ introduces into the molten cryolite one new species, VO_3^- (Na^+ is not a new species as it is a dissociation product of cryolite [10, 11]). In fact, k_{St} is higher than 1 indicating additional interactions in the melt.

The weak inflection point on the liquidus curve of Na_3AlF_6 at $x_{inflection} = 0.52$ indicates the presence of the chemical reaction between components as well.

In order to look into the additional interaction in the melt between cryolite and $NaVO_3$ the quenched samples of the composition $x(NaVO_3) = 0.20$ and $x(NaVO_3) = 0.40$ were prepared and analysed by means of XRD (Fig. 3).

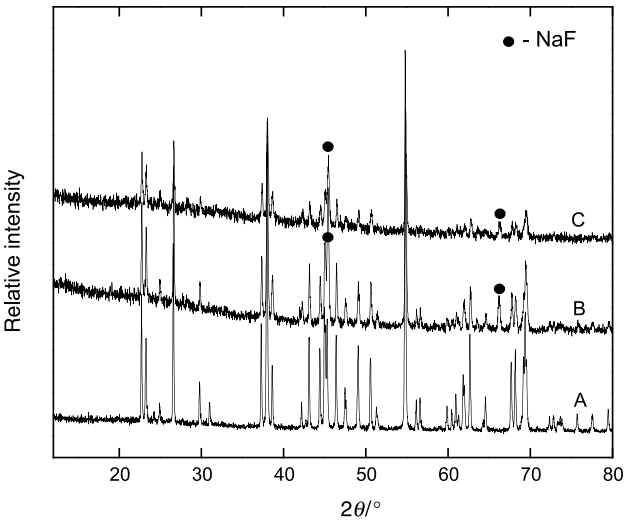

Fig. 3. XRD patterns of quenched mixtures: A = (Na_3AlF_6), B = ($x(NaVO_3) = 0.20$), C = ($x(NaVO_3) = 0.40$)

It can be supposed that during quenching at least some portion of the system remains in the metastable state corresponding to the real structure in the melt. The presence of only cryolite phase (and NaF phase; see below) was observed. Surprisingly, the pattern of crystalline phase of $NaVO_3$ is missing which is in contradiction with the results of XRD patterns of the same composition of the samples from thermal analysis with controlled cooling rate. This observation can be explained by the formation of a glassy phase as $NaVO_3$ belongs to the category of compounds providing amorphous phases after rapid cooling. This is related to the structural properties where alkali metavanadates have infinite chains formed by VO_4 tetrahedra sharing corners [14]. In this respect, they are similar to the silicates. The amorphous feature in the recorded patterns can be observed in the formation of the slightly increased background in the range of 2θ =20–35°. The formation of this amorphous phase is connected with the expected additional interactions, however, the nature of them cannot be deduced from present experiments. This suggestion is supported by the formation of the NaF phase in the XRD patterns of quenched mixtures of Na_3AlF_6–$NaVO_3$.

Conclusions

The thermal analysis showed a high solubility of $NaVO_3$ in molten cryolite. On the other hand, the negative *Gibbs* energy of the reaction between $NaVO_3$ and molten aluminum indicates a high re-

action affinity between these ones (Eq. (1)). Consequently, a decrease of the $NaVO_3$ content in molten cryolite should be expected, analogous to the system Na_3AlF_6-V_2O_5 [4]. This effect will be enhanced in industrial application where the content of vanadium impurities is low.

From thermodynamic and XRD analysis it follows that some additional interactions are expected in the melt, besides simple dissociation of $NaVO_3$ under the formation of Na^+ and VO_3^- ($k_{St} > 1$).

Experimental

Natural hand-picked Na_3AlF_6 from Greenland (melting point: 1009–1011°C), AlF_3 sublimated under vacuum in graphite crucible (min 99.0%), NaF (Merck, 99.9%), $NaVO_3$ (Aldrich, anhydrous, 99.9%), NaCl (Fluka, 99.9%), and KCl (Fluka, 99.9%). All chemicals were dried under vacuum at 150°C for 5 h and handled in a glove box under dry nitrogen atmosphere (Messer, 99.99%).

The liquidus curves in the system Na_3AlF_6–$NaVO_3$ were determined by thermal analysis. Since $NaVO_3$ is hygroscopic, the use of inert atmosphere was of primary importance in the preparation of the samples and during the measurements. 10.000 ± 0.001 g of the mixtures Na_3AlF_6-$NaVO_3$ with known composition were homogenized and transferred into a Pt crucible. The Pt crucible was placed in a vertical resistance furnace, under argon atmosphere (Messer, 99.996%). The temperature was measured using a Pt-PtRh10 thermocouple calibrated with respect to the melting point of known compounds (NaCl, KCl, and NaF). The reproducibility of the measured temperatures was within ±2°C. The used cooling rate was 1.2°C min^{-1}. To collect the XRD patterns a transmission *Stoe Stadi* P diffractometer equipped with a linear PSD and a curved Ge(111) primary beam monochromator was used. XRD patterns were collected within the interval of 10–80° in steps of $2\theta = 0.02°$ using Co $K_{\alpha 1}$ radiation. The samples were mounted between foils.

The investigated mixtures were heated under argon at 1000°C for 1 h in the Pt crucible covered with a Pt lid. The samples were than quenched by immersing the platinum crucibles with the samples into crushed ice. Finally, the samples were collected and powdered.

Acknowledgement

Slovak Grant Agencies (VEGA-2/4071/04, APVT-51-008104) are acknowledged for financial support.

References

[1] Grjotheim K, Krohn C, Malinovský M, Matiašovsky K, Thonstad J (1982) Aluminium Electrolysis, Fundamentals of the Hall-Héroult Process, 2nd ed., Aluminium-Verlag, Düsseldorf, Germany
[2] Thonstad J, Fellner P, Haarberg GM, Híveš J, Kvande H, Sterten Å (2001) Aluminium Electrolysis, Fundamentals of the Hall–Héroult Process, 3rd ed., Aluminium-Verlag, Düsseldorf, Germany
[3] Sterten Å, Solli PA, Skybakmoen E (1998) J Appl Electrochem **28**: 781
[4] Bratland D, Campo JJ, Cho K, Grjotheim K, Thonstad J (1982) Light Metals: 325
[5] Rolin M, Bernard M (1963) Bull Soc Chim France: 1035
[6] Belyaev AI, Rapoport MB, Firsanova LA (1953) Elektrometallurgiya Alyuminiya, Metallurgizdat, Moscow
[7] Goodes CG, Algie SH (1989) Light Metals: 199
[8] Chrenková M, Silný A, Šimko F (2005) Chem Pap **59**: 85
[9] Stortenbeker W (1892) Z Phys Chem **10**: 183
[10] Šimko F, Proks I, Daněk V, Boča M, Chrenková M (2004) Z Phys Chem **218**: 1213
[11] Proks I, Daněk V, Chrenková M, Šimko F, Panek Z (2002) Chem Pap **56**: 71
[12] Sterten A, Mæland I (1985) Acta Chem Scand A39: 241
[13] Barin I (1993) Thermochemical Data of Pure Substances, VCH, Weinheim, Germany
[14] Greenwood NN, Earnshaw A (1984) Chemistry of the Elements, Pergamon Press, London